through MDM2 titration.[7,80] In addition, Goldschneider *et al.* found that p73 promotes the nuclear localization of wild-type p53 in neuroblastoma cells in which p53 is predominantly expressed in cytoplasm.[80] These results suggest that p73 has an ability to enhance the activity of wild-type p53. In contrast, Vikhanskaya *et al.* described that p73 reduces the p53-mediated transcriptional activation through the competition of the same DNA-binding site.[81] These controversial results regarding the effects of p73 on wild-type p53 might be at least in part due to the different cell systems used in those studies.

Recently, it has been shown that p53-dependent apoptosis requires the indirect contribution of at least one other p53 family member, p73 or p63.[5] Thus, it is likely that p73 cooperates with p53 to promote apoptotic cell death. These findings emphasize the functional importance of p73 in the regulation of the DNA damage-induced apoptotic response.

## Role of p73 in neuronal differentiation

Considering that p73-deficient mice in which both TAp73 and ΔNp73 have been deleted, displayed profound developmental defects in their nervous and immune systems including a severe distortion of the hippocampal formation, it is likely that p73 contributes to normal neural development.[8] Indeed, ΔNp73 was expressed predominantly in the developing brain and sympathetic neurons, and p53-dependent neuronal apoptosis was inhibited by ΔNp73.[9] Consistent with this notion, De Laurenzi *et al.* demonstrated that p73 is induced to be accumulated during retinoic acid-mediated neuronal differentiation in neuroblastoma cell lines, whereas p53 levels remained unchanged in response to retinoic acid.[21] Under their experimental conditions, ectopic overexpression of p73 in undifferentiated neuroblastoma cell lines resulted in the induction of neurite extension as well as the expression of neuronal differentiation markers. In contrast, the transcriptionally inactive mutant form of p73 had undetectable effects on the neuronal differentiation. Similar results were also observed during neuronal differentiation in P19 cells exposed to retinoic acid.[46] Of note, Billon *et al.* described that the ectopic expression of p73 induces oligodendrocyte precursor cell (OPC) differentiation, and that ΔNp73 inhibits OPC differentiation in culture.[82] These observations strongly suggest that, in addition to its apoptosis-inducing activity upon DNA damage, p73 plays a pivotal role in the regulation of proper neuronal differentiation.

## Role of p73 in the p53-independent cellular pathway

p53 plays a central role in the regulation of apoptotic cell death in response to DNA damaging agents. p53 function is lost by various mechanisms, including loss of function mutations within the *p53* gene itself or defects in upstream and/or downstream mediators of p53. Recent findings clearly demonstrated that p53-dependent apoptosis in response to DNA damage is impaired in cells lacking both p73 and p63, indicating that p73 and p63 are critical components of the apoptotic response to DNA damage.[5] Accumulating evidence strongly suggests that the pro-apoptotic activity of p73 is regulated through a pathway distinct from that used for p53. As certain cancerous cells were resistant to p53-dependent apoptotic cell death, p73 could be one of several candidate tumor suppressor proteins which can promote apoptosis by p53-independent mechanisms. Previous studies revealed that the exogenous expression of p73 in p53-deficient cells results in significant cell death through apoptosis in a p53-independent manner.[4] It is worth noting that p73 has an ability to promote apoptotic cell death in various pancreatic cells lacking functional p53, which are resistant to wild-type p53 gene transfer.[83] Thus, it is possible that p73 could be particularly useful in treating cancerous cells with non-functional p53.

## What is the difference between p73 and p63?

The overall genomic organization of *p63* is quite similar to that of *p73*; the *p63* gene contains 15 exons.[23] Although *p63* is mapped to human chromosome 3q27–29, a region which is altered in a variety of cancers derived from lung, cervix or ovary, *p63* was infrequently mutated in primary tumors.[2,20] Like p73, p63 gives rise to at least six splicing variants as well as an $NH_2$-terminally truncated form of p63 (ΔNp63) arising from the alternative promoter usage. ΔNp63, a direct transcriptional target of p53, had a dominant negative effect on TAp63.[84] As expected from its structural similarity to p73, p63 can bind to the p53-responsive element and transactivate an overlapping set of p53-regulated genes, thereby inducing cell cycle arrest and/or apoptosis.[2] In contrast to p73, E2F1 did not stimulate the transcription of *p63*, although the putative E2F1-binding sites were found within the *p63* promoter region.[84]

At a sequence level, *p63* is much more similar to *p73* than *p53*, raising the possibility that *p73* or *p63* might be the original *p53* family gene, and that *p53* might be phylogenetically younger.[85] In support of this notion, p73 and p63 contribute to normal development, and p53 holds additional biological properties such as strong tumor suppressor activity. Despite the structural and functional similarities between p73 and p63, knockout phenotypes and the expression patterns of p63 were quite different from those of p73. In sharp contrast to *p73*, whose expression was restricted to the epidermis, sinuses, inner ear and brain, *p63* was predominantly expressed in the epidermis, cervix, urothelium and prostate.[23] Unlike p73-deficient mice, p63-deficient mice exhibited severe defects in limb, cranio-facial and epithelial development.[86,87] For example, p63-deficient mice lacked all squamous epithelia, and displayed severe forelimb truncations. Consistent with these developmental defects, *p63* mutations were detected in children affected by EEC (ectrodactyly, ectodermal dysplasia, and facial clefts) syndrome.[88] Thus, it is likely that p73 and p63 have overlapping and distinct biological activities, and they express their specific functions depending on their unique sites of action.

## Conclusion

p53 and p73 share extensive structural and functional similarities. They have overlapping as well as distinct biological functions. In addition to its potent tumor suppressor function, at least in specific tissues, p73 plays a pivotal role in normal neurogenesis *in vivo*. Similar to

51 Donehower LA, Harvey BL, Slagle BL *et al.* Mice deficient for p53 are developmentally normal but susceptible to spontaneous tumours. *Nature* 1992; **356**: 215–21.
52 Gong J, Constanzo A, Yang H-Q *et al.* The tyrosine kinase c-Abl regulates p73 in apoptotic response to cisplatin-induced DNA damage. *Nature* 1999; **399**: 806–9.
53 Agami R, Blandino G, Oren M, Shaul Y. Interaction of c-Abl and p73α and their collaboration to induce apoptosis. *Nature* 1999; **399**: 809–13.
54 Yuan Z-M, Shioya H, Ishiko T *et al.* p73 is regulated by tyrosine kinase c-Abl in the apoptotic response to DNA damage. *Nature* 1999; **399**: 814–7.
55 Ren J, Datta R, Shioya H *et al.* p73β is regulated by protein kinase Cδ catalytic fragment generated in the apoptotic response to DNA damage. *J Biol Chem* 2002; **277**: 33758–65.
56 Gonzalez S, Prives C, Cordon-Cardo C. p73α regulation by Chk1 in response to DNA damage. *Mol Cell Biol* 2003; **23**: 8161–71.
57 Gaiddon C, Lokshin M, Gross I *et al.* Cyclin-dependent kinases phosphorylate p73 at threonine 86 in a cell cycle-dependent manner and negatively regulate p73. *J Biol Chem* 2003; **278**: 27421–31.
58 Zeng X, Li X, Miller A *et al.* The N-terminal domain of p73 interacts with the CH1 domain of p300/CREB binding protein and mediates transcriptional activation and apoptosis. *Mol Cell Biol* 2000; **20**: 1299–310.
59 Costanzo A, Merlo P, Pediconi N *et al.* DNA damage-dependent acetylation of p73 dictates the selective activation of apoptotic target genes. *Mol Cell* 2002; **9**: 175–86.
60 Mantovani F, Piazza S, Gostissa M *et al.* Pin1 links the activities of c-Abl and p300 in regulating p73 function. *Mol Cell* 2004; **14**: 625–36.
61 Kramer S, Ozaki T, Miyazaki K, Kato C, Hanamoto T, Nakagawara A. Protein stability and function of p73 are modulated by a physical interaction with RanBPM in mammalian cultured cells. *Oncogene* 2005; **24**: 938–44.
62 Leng RP, Lin Y, Ma W *et al.* Pirh2, a p53-induced ubiquitin protein ligase, promotes p53 degradation. *Cell* 2003; **112**: 779–91.
63 Wu L, Zhu H, Nie L, Maki CG. A link between p73 transcriptional activity and p73 degradation. *Oncogene* 2004; **23**: 4032–6.
64 Rossi M, De Laurenzi V, Munarriz E *et al.* The ubiquitin-protein ligase Itch regulates p73 stability. *EMBO J* 2005; **24**: 836–48.
65 Miyazaki K, Ozaki T, Kato C *et al.* A novel HECT-type E3 ubiquitin ligase, NEDL2, stabilizes p73 and enhances its transcriptional activity. *Biochem Biophys Res Commun* 2003; **308**: 106–13.
66 Toh WH, Siddique MM, Boominathan L, Lin KW, Sabapathy K. c-Jun regulates the stability and activity of the p53 homologue, p73. *J Biol Chem* 2004; **279**: 44713–22.
67 Hosoda M, Ozaki T, Miyazaki K *et al.* UFD2a mediates the proteasomal turnover without promoting p73 ubiquitination. *Oncogene* (forthcoming).
68 Marin MC, Jost CA, Irwin MS *et al.* Viral oncoproteins discriminate between p53 and the p53 homolog p73. *Mol Cell Biol* 1998; **18**: 6316–24.
69 Roth J, Konig C, Wienzek S *et al.* Inactivation of p53 but not p73 by adenovirus type 5 E1B 55-kilodalton and E4 34-kilodalton oncoproteins. *J Virol* 1998; **72**: 8510–6.
70 Steegenga WT, Shvarts A, Riteco N, Bos JL, Jochemsen AG. Distinct regulation of p53 and p73 activity by adenovirus E1A, E1B, and E4orf6 proteins. *Mol Cell Biol* 1999; **19**: 3885–94.
71 Dobbelstein M, Wienzek S, Konig C, Roth J. Inactivation of the p53-homologue p73 by the MDM2-oncoprotein. *Oncogene* 1999; **18**: 2101–6.
72 Strano S, Munarriz E, Rossi M *et al.* Physical interaction with Yes-associated protein enhances p73 transcriptional activity. *J Biol Chem* 2001; **276**: 15164–73.
73 Watanabe K, Ozaki T, Nakagawa T *et al.* Physical interaction of p73 with c-Myc and MM1, a c-Myc-binding protein, and modulation of the p73 function. *J Biol Chem* 2002; **277**: 15113–23.
74 Ozaki T, Watanabe K, Nakagawa T *et al.* Function of p73, but not of p53, is inhibited by the physical interaction with RACK1 and its inhibitory effect is counteracted by pRB. *Oncogene* 2003; **22**: 3231–42.
75 Hanamoto T, Ozaki T, Furuya K *et al.* Identification of protein kinase A catalytic subunit β as a novel binding partner of p73 and regulation of p73 function. *J Biol Chem* 2005; **280**: 16665–75.
76 Di Como CJ, Gaiddon C, Prives C. p73 function is inhibited by tumor-derived p53 mutants in mammalian cells. *Mol Cell Biol* 1999; **19**: 1438–49.
77 Marin MC, Jost CA, Brooks LA *et al.* A common polymorphysm acts as intragenic modifier of mutant p53 behaviour. *Nat Genet* 2000; **25**: 47–54.
78 Bergamaschi D, Gasco M, Hiller L *et al.* p53 polymorphysm influences response in cancer chemotherapy via modulation of p73-dependent apoptosis. *Cancer Cell* 2003; **3**: 387–402.
79 Miro-Mur F, Meiller A, Haddada H, May E. p73α expression induces both accumulation and activation of wt-p53 independent of the p73α transcriptional activity. *Oncogene* 2003; **22**: 5451–6.
80 Goldschneider D, Blanc E, Raguenez G *et al.* When p53 needs p73 to be functional-forced p73 expression induces nuclear accumulation of endogenous p53 protein. *Cancer Lett* 2003; **197**: 99–103.
81 Vikhanskaya F, D'Incalci M, Broggini M. p73 competes with p53 and attenuates its response in a human ovarian cancer cell line. *Nucl Acids Res* 2000; **28**: 513–9.
82 Billon N, Terrinoni A, Jolicoeur C *et al.* Roles for p53 and p73 during oligodendrocyte development. *Development* 2004; **131**: 1211–20.
83 Rodicker F, Putzer BM. p73 is effective in p53-null pancreatic cancer cells resistant to wild-type TP53 gene replacement. *Cancer Res* 2003; **63**: 2737–41.
84 Waltermann A, Kartasheva NN, Dobbelstein M. Differential regulation of p63 and p73 expression. *Oncogene* 2003; **22**: 5686–93.
85 Strano S, Rossi M, Fontemaggi G *et al.* From p63 to p53 across p73. *FEBS Lett* 2001; **490**: 163–70.
86 Mills AA, Zheng B, Wang X-J, Vogel H, Roop DR, Bradley A. p63 is a p53 homologue required for limb and epidermal morphogenesis. *Nature* 1999; **398**: 708–13.
87 Yang A, Schweitzer R, Sun D *et al.* p63 is essential for regenerative proliferation in limb, craniofacial and epithelial development. *Nature* 1999; **398**: 714–8.
88 Celli J, Duijf P, Hamel BCJ *et al.* Heterozygous germline mutations in the p53 homolog p63 are the cause of EEC syndrome. *Cell* 1999; **99**: 143–53.

Journal of Pediatric Surgery (2005) 40, 359–363

ELSEVIER

Journal of Pediatric Surgery

www.elsevier.com/locate/jpedsurg

# Profile of neuroblastoma detected by mass screening, resected after observation without treatment: results of the Wait and See pilot study

**Takaharu Oue[a,*], Masami Inoue[b], Akihiro Yoneda[c], Akio Kubota[c], Hiroomi Okuyama[c], Hisayoshi Kawahara[c], Masanori Nishikawa[d], Masahiro Nakayama[e], Keisei Kawa[b]**

[a]*Department of Pediatric Surgery, Jichi Medical School, Minamikawachi-machi, Tochigi, 329-0498, Japan*
[b]*Department of Pediatrics, Osaka Medical Center and Research Institute for Maternal and Child Health, Izumi, Osaka, 565-0871, Japan*
[c]*Department of Pediatric Surgery, Osaka Medical Center and Research Institute for Maternal and Child Health, Izumi, Osaka, 565-0871, Japan*
[d]*Department of Radiology, Osaka Medical Center and Research Institute for Maternal and Child Health, Izumi, Osaka, 565-0871, Japan*
[e]*Department of Pathology, Osaka Medical Center and Research Institute for Maternal and Child Health, Izumi, Osaka, 565-0871, Japan*

**Index words:**
Neuroblastoma;
Mass screening;
Spontaneous regression;
Observation

**Abstract**

**Background/Purpose:** Neuroblastoma (NB) detected by mass screening (MS) usually shows favorable prognosis and sometimes regresses spontaneously. Therefore, the authors started an observation program for these patients to avoid overtreatment. In this study, the authors analyzed the profile of NB resected after observation to elucidate the nature of NB detected by MS.

**Methods:** Between 1994 and 2004, 22 NB patients matched the following criteria and entered the observation program after obtaining informed consent: stage I or II, less than 5 cm in diameter, and without involvement of large vessels or organs. If increase in size, elevation of tumor markers, or evidence of metastasis was observed, the tumor was immediately resected.

**Results:** Thirteen (59%) of 22 cases showed spontaneous regression. In the remaining 9 cases, tumors were resected because of parents' request, increase in size, and/or elevation of tumor markers. Four tumors had at least one unfavorable biologic feature, and 3 of them had more than 2. According to Shimada's system, 2 had unfavorable histology. One was diploid tumor, 3 had 1p deletion, and Trk-A expression was low in 4 tumors. All patients survived without evidence of recurrence.

**Conclusions:** The observation program has shown that at least one third of the NB detected by MS regressed spontaneously. On the other hand, MS may detect some cases with unfavorable tumor in early stage, which benefit from screening.



Presented at the 51st Annual Congress of the British Association of Paediatric Surgeons, Oxford, England, July 27-30, 2004.

* Corresponding author. Department of Pediatric Surgery, Jichi Medical School, Minamikawachi-machi, Tochigi-ken, 329-0498, Japan. Tel.: +81 285 58 7371; fax: +81 285 44 3234.
*E-mail address:* oue@jichi.ac.jp (T. Oue).

0022-3468/05/4002-0012$30.00/0 
doi:10.1016/j.jpedsurg.2004.10.062

The prognosis of neuroblastoma (NB) in younger than 1 year is much better than that older than 1 year. In 1985, Japanese nationwide mass screening (MS) using urinary vanillyl mandelic acid (VMA) and homovanillic acid (HVA) for 6-month-old infants was started to improve the prognosis of this tumor [1]. Since then, more than 2000 patients with NBs were discovered and treated. Their prognosis was extremely good: more than 97% of them are alive [2]. Moreover, the majority of the NBs in MS group were biologically favorable even in advanced stages [3]. Recent reports have also shown that NB detected by MS sometimes regresses spontaneously [4,5]. Although the incidence of NB has remarkably increased after introduction of MS, several reports suggest that the number of advanced NB patients older than 1 year has not decreased substantially [3]. These findings indicate that MS has detected tumors that otherwise may have regressed spontaneously without recognition [4,5]. Therefore, we started an observation program in the limited cases to avoid overtreatment and to estimate how frequently regression occurs (Wait and

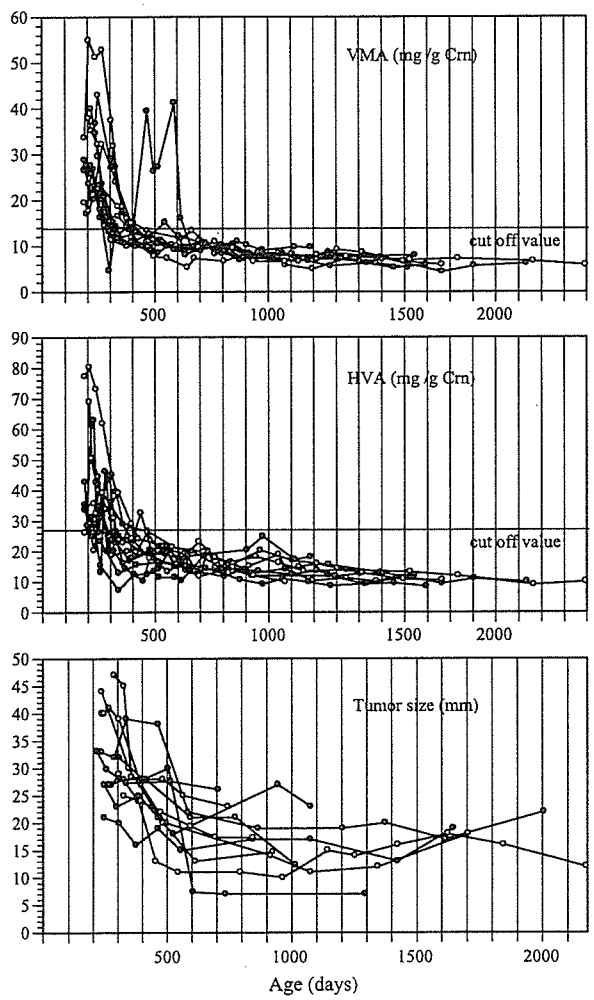


**Fig. 1** Changes in levels of VMA and HVA, and tumor size in regressed cases.

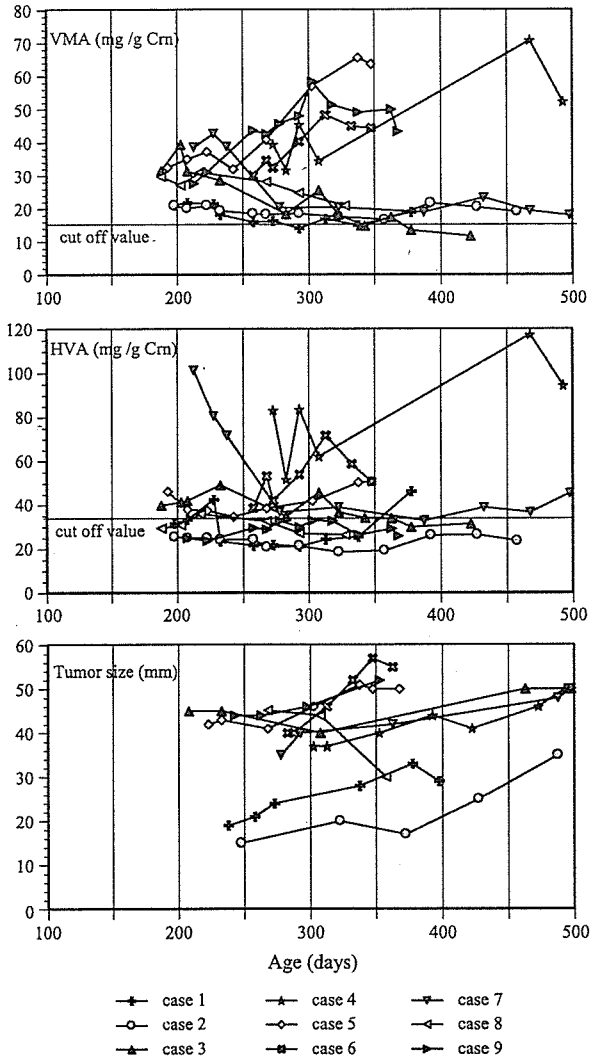


**Fig. 2** Changes in levels of VMA and HVA, and tumor size in regressed cases. The cutoff values of urinary VMA/HVA levels were 12.6 and 27.0 mg/g Crn, respectively.

See pilot study) in June 1994 [6]. Our preliminary results have shown that at least 60% of NB cases who entered our observation program regressed spontaneously [6]. In this study, we analyzed the profile of NB resected after observation to elucidate the nature of NB detected by MS.

## 1. Patients and methods

The details of our observation program have been described previously [6]. The entry criteria were as follows: (1) stage I and II [7], (2) less than 5 cm in diameter, (3) no involvement of large vessels or organs and surgical resection is not difficult, and (4) parents' informed consent. The patients were strictly followed up without receiving any treatment. If increase in size, elevation of tumor markers, or evidence of metastasis was observed, the tumor was

**Table 1** Neuroblastoma resected after observation

| Case | Stage | Origin | Initial | | | Preoperative | | | Reason of interruption | Obs days | Age at ope (mo) |
|---|---|---|---|---|---|---|---|---|---|---|---|
| | | | VMA | HVA | Size | VMA | HVA | Size | | | |
| 1 | IVs | Lt retro | 21.1 | 31.6 | 19 | 19.0 | 46.3 | 33 | Size ↑, marker ↑ | 199 | 13 |
| 2 | I | Lt retro | 21.0 | 25.5 | 15 | 19.1 | 23.7 | 25 | Size ↑, parents' request ↑ | 291 | 16 |
| 3 | I | Lt adrenal | 31.5 | 39.9 | 40 | 11.7 | 31.5 | 50 | Size ↑ | 309 | 16 |
| 4 | I→III | Lt adrenal | 39.5 | 83.3 | 37 | 52.4 | 94.5 | 50 | Size ↑, LN meta ↑ | 226 | 16 |
| 5 | I→II | Rt adrenal | 32.5 | 46.3 | 42 | 63.7 | 50.9 | 50 | Size ↑, marker ↑ | 174 | 11 |
| 6 | I | Lt adrenal | 30.0 | 38.7 | 40 | 44.4 | 50.6 | 57 | Size ↑, marker ↑ | 96 | 11 |
| 7 | II | Rt retro | 38.6 | 101.5 | 35 | 18.0 | 45.4 | 50 | Size ↑ | 300 | 16 |
| 8 | I | Rt adrenal | 29.7 | 29.5 | 45 | 20.9 | 26.7 | 40 | Parents' request | 172 | 11 |
| 9 | I→III | Rt retro | 27.6 | 25.0 | 44 | 43.3 | 26.0 | 52 | Size ↑ | 159 | 12 |

Size indicates longer diameter (mm); stage, Evans' staging system [7]; Lt, left; Rt, right; retro, retroperitoneum; LN meta, lymph node metastasis; obs, observation; ope, operation.

resected immediately. Biological features of the tumor were identified: Shimada's histological features [7], amplification of N-*myc* (Southern blotting, SRL Inc, Tokyo, Japan), 1p deletion (FISH, Otsuka Assay Laboratory, Tokyo, Japan), and expression of Trk-A (immunohistochemistry) [8]. Between June 1994 and March 2004, 43 patients with NB detected by MS were admitted to our hospital, and 22 (51 %) of them matched the criteria and were enrolled in the observation program. They included 11 boys and 11 girls. Age at diagnosis ranged from 7 to 11 months. Origins of the tumors were adrenal grand in 15 and retroperitoneal paraganglion in 7. Seventeen cases were in stage I, and 3 in stage II. Two patients in stage IV were also enrolled in the study, because the parents refused any treatment.

## 2. Results

Thirteen (59%) of 22 cases showed spontaneous regression and continued the observation program. The observation periods ranged from 15 to 116 months until May 2004. Urinary levels of VMA and HVA decreased and normalized within 18 months in all cases except one (Fig. 1). The tumor size (maximum diameter) was decreased to 0.7 to 2 cm within 3 years in all the cases; however, no tumor has disappeared (Fig. 1). In the remaining 9 (41%) cases, tumor resection was performed in 96 to 309 days after initial screening. In 2 cases, parents decided to stop the observation; therefore, the tumors were resected after 291- and 172-day observation. The remaining 7 tumors were resected because of increase in size and/or elevation of tumor markers (Fig. 2). In 2 cases (cases 4 and 5), lymph node metastases were observed at operation, resulting in the upgrading of the tumor stage from I to II and I to III, respectively. In case 9, tumor growth resulted in the upgrading of stage from I to III. The profile of the resected cases is listed in Tables 1 and 2. Four tumors (cases 2, 3, 7, and 8) showed differentiation to ganglioneuroblastoma. Biological features of the 9 resected tumors were listed in Table 2. According to Shimada's system, 7 were favorable, and 2 were unfavorable. DNA content was aneuploid in 7 tumors and diploid in one. Three of them had 1p deletion. Trk-A expression was low in 4 cases. Two cases (cases 6 and 7) showed biological heterogeneity in the tumor. No tumor showed N-*myc* amplification. Four (44%) tumors had at least one unfavorable biologic feature, and 3 of 4 tumors had more than 2 features. All tumors were resected completely without major surgical complication. Two of

**Table 2** Neuroblastoma resected after observation

| Case | His | Shimada's classification | N-*myc* (copy) | DNA ploidy | 1p deletion | Trk-A expression | Operative procedure | Post operative chemotherapy |
|---|---|---|---|---|---|---|---|---|
| 1 | NB | Unfavorable | I | A | − | Low | Open | + |
| 2 | GNB | Favorable | I | A | − | High | Open | − |
| 3 | GNB | Favorable | I | ND | − | High | Laparoscopic | − |
| 4 | NB | Favorable | I | A | − | High | Open | + |
| 5 | NB | Favorable | I | A | + | Low | Open | − |
| 6* | NB | Favorable | I | A/D | + | High/low | Open | − |
| 7* | GNB | Unfavorable | I | A/A | +/− | Low/low | Open | + |
| 8 | GNB | Favorable | I | A | ND | ND | Laparoscopic | − |
| 9 | NB | Favorable | I | A | − | ND | Open | + |

His indicates histology; GNB, ganglioneuroblastoma; ND, not detected; A, aneuploid; D, diploid.
* Showed intratumoral heterogeneity.

them were resected laparoscopically. Postoperative chemotherapy was performed in 4 cases who had stage III tumor and/or unfavorable prognostic factors. All patients survived without evidence of recurrence.

## 3. Discussion

In the presented series, among 43 NBs detected by MS, 22 have entered the observation program, and 13 tumors regressed spontaneously. Therefore, tumors are expected to regress at least in 59% of the patients who fulfilled our observation program or in 29% of all the patients detected by MS. Moreover, 5 of the 9 resected tumors had favorable biologic feature, which indicate that they have possibility of spontaneous regression if observation was continued. Therefore, the incidence of spontaneous regression should be higher. Similar observation trials were made at other institutes; Nishihira et al [5] reported that 17 (65%) tumors of 26 patients who were enrolled in their observation program regressed. Yamamoto et al [4] reported that 92% of the observed tumors or 44% of all the tumors identified by MS have spontaneously regressed. These results suggested that at least one third of the NB detected by MS might regress spontaneously. To avoid the overtreatment, several trials have been introduced including laparoscopic surgery [9] and reduction of chemotherapy [5]. We consider that observation program is most effective to avoid the unnecessary treatment.

Most of screened NBs were biologically favorable. However, there was a small group with biologically unfavorable factors, such as diploid DNA content, chromosomal pattern with 1p deletion, lower Trk-A expression, and N-*myc* amplification. Suita et al reported that 5 of 285 NBs detected by MS had amplified N-*myc* oncogene, 4 of 74 showed unfavorable Shimada's histological findings, and 3 of 33 had an unfavorable DNA ploidy pattern [3]. Therefore, MS may detect 2 biologically different groups, described as favorable and unfavorable. The unfavorable tumors may progress and/or disseminate in the future. Mass screening enables the cases with unfavorable tumor to undergo early treatment; therefore, these cases may benefit from MS. The favorable and unfavorable group can be identified only after analysis for the surgically removed tumor specimens. Therefore, identification of new prognostic factors that could distinguish the regressing tumor without surgery is required. Our examinations of the resected tumors after observation revealed high incidence of unfavorable biologic factors and upgrading of the tumor stage. Four (44%) of 9 resected tumors had at least one unfavorable biological feature. This percentage is much higher than reported percentage (0% to 20%) among all of the NBs detected by MS [3,10]. These findings suggest that unfavorable tumor may grow in size; therefore, they can be distinguished from the regressing tumors and be resected if they enter the observation program.

To clarify the benefits of MS in public health, we should prove whether MS decreases the number of advanced tumors and improves the survival. Several reports suggested that MS did not improve the overall mortality rate of NB [3]. Moreover, the results of the present study have proven that MS detects a considerable number of regressing tumors. Treatment of the regressing tumors may extremely harm the significance and cost benefit of MS, because the patients with regressing tumors had not received any treatment if MS would not have detected them. Based on the information obtained so far, the MS for NB at 6 months of age probably should not contribute to the public health. Therefore, Japanese Ministry of Health and Welfare has decided to discontinue the MS for NB at 6 months of age in April 2004. At the same time, our observation program at 6 months of age was also closed.

The optimal time for MS should be the point at which NB regressing spontaneously can no longer be detected, but more aggressive tumors can be found. Our observation program may determine the optimal timing of screening. Urinary VMA and HVA levels were normalized within 18 months in most of the regressed cases (Fig. 1). On the other hand, in the patients whose tumor increased in size, VMA and HVA levels were over the cutoff value at the time of operation. These findings suggest that screening in age around 18 months may be more effective; most of the favorable tumor has regressed, and unfavorable tumor should be detected. Now we are planning to start the new MS program for 18-month-old infants in Osaka prefecture, expecting to clarify whether MS in older age has benefit or not.

## Acknowledgment

The authors thank Dr Tanaka of National Kure Hospital for detection of Trk-A expression.

## References

[1] Sawada T, Matsumura T, Kawakatsu H, et al. Long-term effects of mass screening for neuroblastoma in infancy. Am J Pediatr Hematol/Oncol 1991;13:3-7.

[2] Matsumura T, Shikata T, Sawada T. Treatment modality for neuroblastoma infants in Japan: retrospective analysis and future directions. Proceedings of the 31st American Society of Clinical Oncology. J Clin Oncol 1995;14:456.

[3] Suita S, Zaizen Y, Sera Y, et al. Mass screening for neuroblastoma: quo vadis? A 9-year experience from the Pediatric Oncology Study Group of the Kyushu area in Japan. J Pediatr Surg 1996;31:555-8.

[4] Yamamoto K, Hanada R, Kikuchi A, et al. Spontaneous regression of localized neuroblastoma detected by mass screening. J Clin Oncol 1998;16:1265-9.

[5] Nishihira H, Toyoda Y, Tanaka Y, et al. Natural course of neuroblastoma detected by mass screening: 5-year prospective study at a single institution. J Clin Oncol 2000;18:3012-7.

[6] Yoneda A, Oue T, Imura K, et al. Observation of untreated patients with neuroblastoma detected by mass screening: a "wait and see" pilot study. Med Pediatr Oncol 2001;36:160-2.

[7] Evans AE, D'Angio GJ, Randolph J. A proposed staging for children with neuroblastoma. Children's Cancer Study Group A. Cancer 1995;27:374-8.
[8] Shimada H, Chatten J, Newton HW, et al. Histologic prognostic factors in neuroblastic tumors; Definition of subtypes of ganglioneuroblastoma and an age-linked classification of neuroblastoma. J Natl Cancer Inst 1984;73:405-16.
[9] Iwanaka T, Arai M, Ito M, et al. Surgical treatment for abdominal neuroblastoma in the laparoscopic era. Surg Endosc 2001;15:751-4.
[10] Tanaka T, Sugimoto T, Sawada T. Prognostic discrimination among neuroblastomas according to Ha-ras/Trk A gene expression: a comparison of the profiles of neuroblastomas detected clinically and those detected through mass screening. Cancer 1998;83:1626-33.

Pediatr Surg Int (2005) 21: 29–33
DOI 10.1007/s00383-004-1258-8

ORIGINAL ARTICLE

Hideki Soh · Masafumi Wasa · Hong-Sheng Wang
Masahiro Fukuzawa

# Glutamine regulates amino acid transport and glutathione levels in a human neuroblastoma cell line

Published online: 11 September 2004


**Abstract** Both amino acid transport and glutathione play a key role in regulating cancer cell growth. Glutamine can serve as an important ATP source for cancer cells, and it can supply glutamate, a precursor for the synthesis of glutathione, by the hydrolysis of glutamine. We examined the effects of glutamine concentrations [2 mM (control), 400 μM, 200 μM, and 0 μM] on cell growth, amino acid transport, and glutathione levels in a human neuroblastoma cell line, SK-N-SH, by using cell culture technique. Cell growth rates were dependent on glutamine concentrations in culture media. Glutamate transport significantly increased in glutamine-deprived groups, and this increase was remarkable in lower glutamine groups (200 μM and 0 μM glutamine). Glutamine deprivation resulted in a significant decrease in glutathione levels by 20% compared with control, but glutathione in 0 μM glutamine was maintained with the same levels found in 400 μM and 200 μM glutamine. DNA and protein synthesis correlated directly with glutamine concentrations in culture media. Our results suggest that glutamine mediates neuroblastoma cell proliferation by regulating amino acid transport and glutathione synthesis, both when sufficient nutrients are present and when key nutrients such as glutamine are in limited supply.

**Keywords** Glutamine · Amino acid transport · Glutathione · Neuroblastoma

## Introduction

Malignant cells display uncontrolled rates of cellular proliferation and require an increased supply of precursor amino acids to support key biosynthetic pathways [1]. As a result, these cells have very efficient transport systems and can transport amino acid across their plasma membranes faster than normal cells can [1]. Glutamine provides nitrogen for a number of important precursors for macromolecule synthesis, including purines, pyrimidines, amino sugars, and some amino acids [2]. In addition, it is an important fuel for cancer cells. It has been shown for cancer cells that both cell growth rates and DNA and protein biosynthesis correlate directly with the concentration of glutamine in culture media [3].

Oxidative stress plays an important role in cancer growth and progression [4]. Glutathione, which serves as a major store of cellular reducing equivalents, is of critical importance to tumor cells, affecting their ability to withstand oxidative attack and their chemosensitivity and radiation sensitivity [5]. Tumor glutathione metabolism also regulates the metastatic behavior of malignant cells [6]. Glutathione is a tripeptide composed of glutamate, glycine, and cysteine. Glutamine metabolism can supply glutamate, a precursor for the synthesis of glutathione, by the hydrolysis of glutamine via the enzyme glutaminase [7]. Abcouwer reported that intracellular glutathione levels dropped rapidly when breast cancer cells were deprived of extracellular glutamine [8].

Neuroblastomas are biologically remarkable in that some regress spontaneously without chemotherapy, and spontaneous and induced maturation is seen with significant frequency [9]. Although many tumor markers have been investigated with respect to the biology of neuroblastomas, a definitive and consistent causal pattern for neuroblastomas' diverse behavior and variable biology is still unexplained.

Because of the potential role of glutamine as a mediator of tumor growth and glutathione production, we hypothesized that glutamine mediates cancer cell growth by regulating amino acid transport activity and glutathione levels, both when sufficient nutrients are present and when key nutrients such as glutamine are in limited supply. The purpose of this study was to examine the effects of glutamine deprivation on amino acid

H. Soh · M. Wasa (✉) · H.-S. Wang · M. Fukuzawa
Department of Pediatric Surgery,
Osaka University Graduate School of Medicine,
2-2 Yamadaoka, Suita, 565-0871 Osaka, Japan
E-mail: wasa@pedsurg.med.osaka-u.ac.jp
Tel.: +81-6-68793753
Fax: +81-6-68793759

transport and glutathione levels in an SK-N-SH human neuroblastoma cell line. In addition, we studied the effects of glutamine deprivation on DNA and protein biosynthesis.

## Materials and methods

### Chemicals

Radiolabeled amino acids ($^3$H-L-glutamine, $^3$H-L-glutamate, and $^3$H-L-leucine) and $^3$H-thymidine were obtained from Amersham (Arlington Heights, IL, USA). Cell culture media were from GIBCO/BRL (Gaithersburg, MD, USA). Amino acids and all biochemicals were purchased from Sigma Chemical (St. Louis, MO, USA), and fetal bovine serum was from JRH Biosciences (Lenexa, KS, USA). Tissue culture plates were obtained from Corning (New York, NY, USA). Neuroblastoma cell line, SK-N-SH, was provided by Dr. Tadao Ohno (RIKEN Cell Bank, Tsukuba, Japan).

### Cell culture

Neuroblastoma cells were cultured at 37ºC under a humidified atmosphere of 5% $CO_2$/95% air. The cells were maintained in Dulbecco's modified Eagle's medium (DMEM) supplemented with 2 mM L-glutamine, 10% fetal bovine serum (FBS), 1,000 units/ml penicillin, and 1,000 units/ml streptomycin. The culture medium was changed every 3 days until cells were confluent, at which point the cells were used for experiments.

### Cell growth measurement

The effect of glutamine concentration on cell growth was determined. Cells were seeded at a density of $1\times10^5$ cells/ml (1 ml/well) into 12-well tissue culture plates. After 24 h, the culture medium was removed and changed to glutamine-free DMEM supplemented with 10% FBS plus various concentrations of glutamine (2 mM, 400 μM, 200 μM, and 0 μM). After 2 days, cells were detached from the plate with trypsin and counted with a hemocytometer. Cell growth in 2 mM glutamine was chosen as the control.

### Measurement of amino acid transport

Cells were seeded into 24-well tissue culture plates (0.5 ml/well) and maintained in DMEM supplemented with 2 mM glutamine and 10% FBS. After getting 100% cell confluence, the culture medium was removed and changed to DMEM supplemented with 10% FBS plus various concentrations of glutamine (2 mM, 400 μM, 200 μM, and 0 μM). Amino acid transport was measured at 24 h.

Amino acid transport was measured by the cluster tray method of Gazzola et al. [10]. Before the transport assays, the cells were rinsed twice with warm sodium-free Krebs-Ringer phosphate buffer (CholKRP, which was made by replacing the corresponding sodium salts with choline chloride and choline phosphate) to remove extracellular sodium and amino acids. The transport of radiolabeled amino acid (5 μCi $^3$H-amino acid/ml) was performed for 1 min at 37ºC at 10 μmol/l unlabeled amino acid in both sodium Krebs-Ringer Phosphate (NaKRP) and CholKRP buffers. The transport reaction was terminated by discarding the uptake buffer and rinsing the cells three times with ice-cold buffer (2 ml/well/rinse). The wells containing the cells were allowed to dry and were solubilized in 200 μl of 0.2 N NaOH/0.2% sodium dodecyl sulfate solution. One hundred μl of the cell extract was neutralized with 10 μl 2 N HCL and subjected to scintillation spectrophotometry. The remaining 100 μl in each well was used for the protein assay by the bicinchoninic acid protein method [11].

The sodium-dependent transport values were obtained by subtracting the transport values in CholKRP from those in NaKRP. Saturable sodium-independent transport values were determined in CholKRP by subtracting the values in the presence of excess (10 mM) unlabeled amino acid from those in its absence.

### Measurement of DNA and protein synthesis

To determine DNA and protein synthesis, we measured the incorporation of $^3$H-thymidine and $^3$H-leucine, respectively, into acid-insoluble material. Cells were seeded in 24-well cluster trays (0.5 ml/well). After getting 100% cell confluence, the medium was removed and replaced with DMEM plus 10% FBS and various concentrations of glutamine (2 mM, 400 μM, 200 μM, and 0 μM). After 24 h, $^3$H-thymidine and $^3$H-leucine (1 μCi/ml) were added to the culture medium, and cells were incubated for 2.5 h at 37ºC. The assay was terminated after 2.5 h, when the cells were washed twice with phosphate-buffered saline (PBS) and fixed by washing three times with ice-cold 10% trichloroacetic acid. Thereafter, cells were rinsed twice with 70% and 95% ethanol, respectively. They were allowed to dry and solubilized in 200 μl of 0.2 N NaOH/0.2% sodium dodecyl sulphate solution. Radioactivity and protein content were measured by the same procedures described for amino acid transport measurements.

### Measurement of glutathione

To determine glutathione levels, equal number of cells was seeded in each 100-mm dishes. After getting 100% cell confluence, the medium was removed and replaced with DMEM plus 10% FBS and various concentrations of glutamine (2 mM, 400 μM, 200 μM, and 0 μM). After 24 h, cells were rinsed twice with PBS and

were detached from the plate with trypsin. They were centrifuged at 500×g for 5 min, and the cell pellet was suspended in 0.2 ml of PBS. The suspension was stored at −80°C until use. The samples were allowed to thaw and were refrozen once more at −80°C before being thawed for use in the assay (two rounds freeze/thaw). Glutathione activity of the cell lysate was measured colorimetrically using the Bioxytech GSH-420 (OXIS International, Portland, OR, USA). Protein concentrations in lysates were determined by the method described for the amino acid transport measurement.

Data (mean ± standard deviation) were analyzed and compared with one-way analysis of variance with post-hoc Turkey-Kramer. A $p$-value $<0.05$ was considered statistically significant.

## Results

### Effects of glutamine concentration on cell growth

As shown in Fig. 1, cell growth rates were dependent on glutamine concentrations. Cell number significantly decreased in the glutamine-deprived groups compared with control, and significant differences were found among the four groups ($p<0.01$).

### Effects of glutamine deprivation on glutamine and glutamate transport

The transport of glutamine and glutamate was linear for at least 3 min, and $Na^+$-dependent glutamine and $Na^+$-dependent glutamate uptake represented 95% and 70% of total uptake, respectively. Therefore, 1-min assays of glutamine and glutamate transport were chosen for subsequent experiments. As shown in Fig. 2, $Na^+$-dependent glutamine transport significantly decreased in 200-μM (2418 ± 267 pmol/mg protein/min) and 0-μM (1909 ± 92 pmol/mg protein/min) glutamine compared with control (3480 ± 226 pmol/mg protein/min) and 400 μM (3366 ± 84 pmol/mg protein/min) glutamine ($p<0.01$). There was a significant decrease in 0-μM glutamine compared with 200-μM glutamine ($p<0.05$).

Fig. 3 shows the effects of glutamine deprivation on total, $Na^+$-dependent, and $Na^+$-independent glutamate transport. Total and $Na^+$-independent glutamate

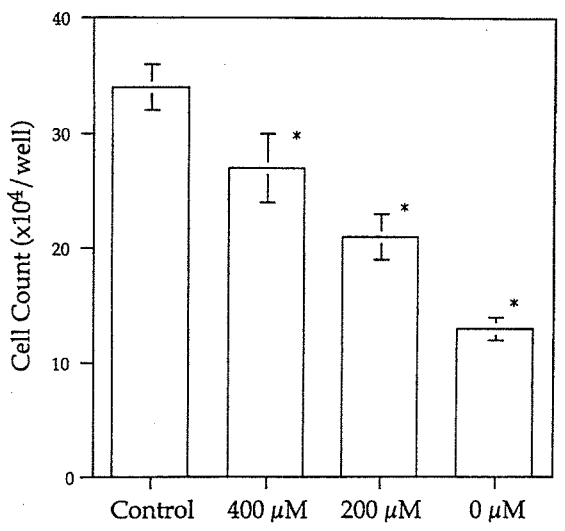


**Fig. 1** Effects of glutamine deprivation on cell growth after 2 days. Data are presented as mean ± standard deviation of triplicate determinations. Control represents 2 mM glutamine. *$p<0.01$ vs. other three groups

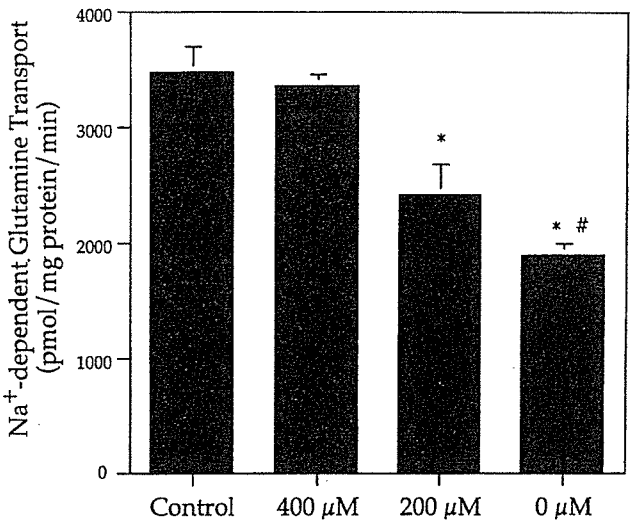


**Fig. 2** Effects of glutamine deprivation on $Na^+$-dependent glutamine transport after 24 h. Data are means ± standard deviation of quadruplicate determinations. *$p<0.01$ vs. control (2 mM glutamine), 400 μM glutamine, #$p<0.05$ vs. 200 μM glutamine

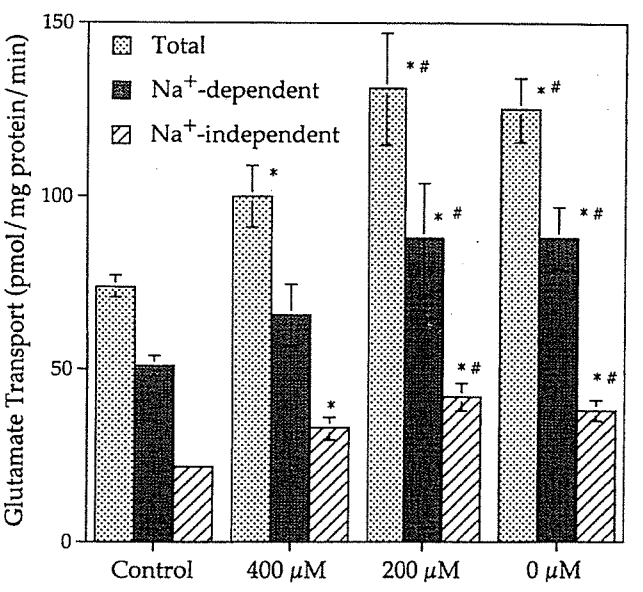


**Fig. 3** Effects of glutamine deprivation on total, $Na^+$-dependent, and $Na^+$-independent glutamate transport after 24 h. Data are means ± standard deviation of quadruplicate determinations. *$p<0.01$ vs. control (2 mM glutamine), #$p<0.05$ vs. 400 μM glutamine

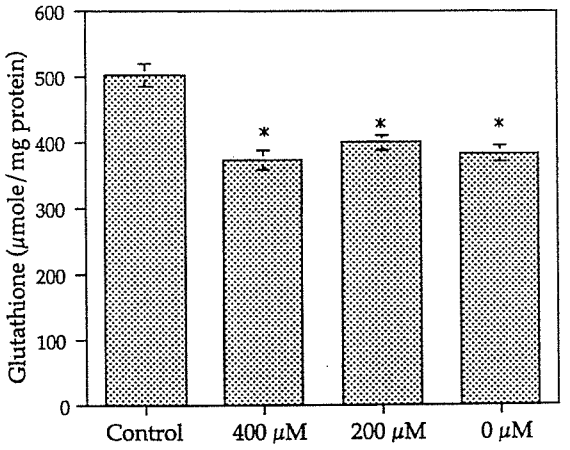


**Fig. 4** Effects of glutamine deprivation on glutathione levels after 24 h. Data are presented as mean ± standard deviation of triplicate determinations. *$p < 0.01$ vs. control (2 mM glutamine)

transport significantly increased in 400-μM (total, 100 ± 9; $Na^+$-independent, 33 ± 3 pmol/mg protein/min), 200-μM (total, 131 ± 16; $Na^+$-independent, 42 ± 4 pmol/mg protein/min), and 0-μM (total, 125 ± 9; $Na^+$-independent, 38 ± 3 pmol/mg protein/min) glutamine compared with control (total, 74 ± 3; $Na^+$-independent, 22 ± 3 pmol/mg protein/min) ($p < 0.01$). $Na^+$-dependent glutamate transport significantly increased in 200-μM (88 ± 16 pmol/mg protein/min) and 0-μM (88 ± 9 pmol/mg protein/min) glutamine compared with control (51 ± 3 pmol/mg protein/min) ($p < 0.01$). Total, $Na^+$-dependent, and $Na^+$-independent glutamate uptake in 200-μM and 0-μM glutamine significantly increased compared with 400-μM glutamine ($p < 0.05$). There were no significant differences between 200-μM and 0-μM glutamine.

### Effects of glutamine deprivation on glutathione levels

As shown in Fig. 4, there was a significant decrease in glutathione levels in 400-μM (375 ± 15 μMole/mg protein), 200-μM (400 ± 12 μMole/mg protein), and 0-μM (383 ± 13 μMole/mg protein) glutamine compared with control (503 ± 18 μMole/mg protein, $p < 0.01$), but no significant differences were found among the three glutamine-deprived groups.

### Effects of glutamine deprivation on DNA and protein synthesis

Glutamine deprivation resulted in remarkable decreases in $^3H$-thymidine incorporation, with significant differences among the four groups (control, 39228 ± 3662; 400 μM, 31925 ± 1764; 200 μM, 23256 ± 1666; 0 μM, 13668 ± 970 cpm/mg protein/hr, $p < 0.01$). $^3H$-leucine incorporation significantly decreased in glutamine-deprived groups (400 μM, 977 ± 66; 200 μM, 814 ± 29; 0 μM, 771 ± 61 cpm/mg protein/hr) compared with control (1104 ± 50 cpm/mg protein/h) ($p < 0.01$), and a significant decrease was found in 200-μM and 0-μM glutamine compared with 400-μM glutamine ($p < 0.01$) (Fig. 5).

## Discussion

SK-N-SH neuroblastoma cells responded to glutamine deprivation by increasing total, $Na^+$-dependent, and $Na^+$-independent glutamate transport, although glutamine deprivation resulted in the decrease of glutamine transport. The increase in glutamate transport was remarkable in lower glutamine levels. The adaptive increase in amino acid transport elicited by glutamine deprivation has already been reported [12–14]. We have shown the adaptive increase of leucine (system L) and Me-AIB [2-(methylamino) isobutyric acid, a substrate for system A] transport in glutamine-deprived SK-N-SH [15]. Because glutamine is used in several disparate metabolic pathways, SK-N-SH neuroblastoma cells may replace metabolic intermediates normally provided by glutamine with the carbon skeletons and nitrogen of other amino acids when the glutamine availability is limited.

Glutamate is formed by the hydrolysis of glutamine via the enzyme glutaminase and transamination

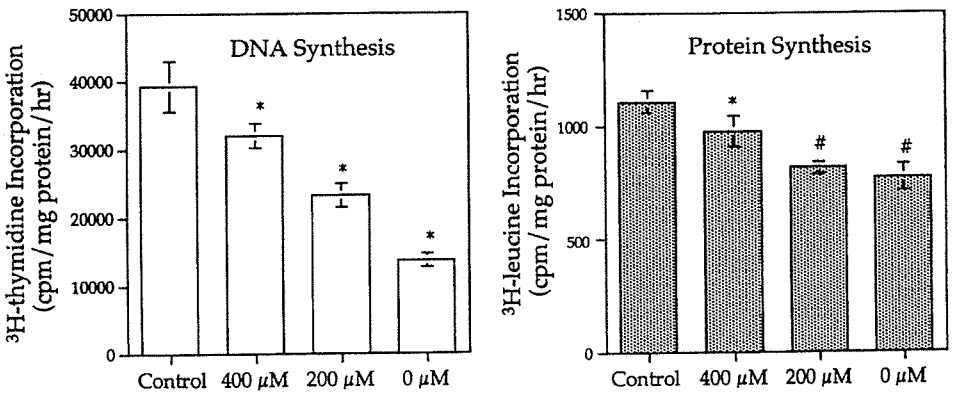


**Fig. 5** Effects of glutamine deprivation on $^3H$-thymidine (DNA synthesis) and $^3H$-leucine (protein synthesis) incorporation after 24 h. Data are presented as mean ± standard deviation of quadruplicate determinations. *$p < 0.01$ vs. other three groups, #$p < 0.05$ vs. control (2 mM glutamine), 400 μM glutamine

reactions that use glutamine as an amine donor. Therefore, glutamine provides a major source for intracellular production of glutamate, a precursor of glutathione. High intracellular glutathione levels in tumors have been associated with high proliferation rates [16] and drug resistance [17]. For example, intracellular glutathione levels are 2.6–2.8-fold higher in renal cell carcinoma than those in the renal cortex [4]. In the present study, intracellular glutathione levels were maintained in 0-μM glutamine with the same levels found in 400-μM and 200-μM glutamine, although glutamine deprivation resulted in the decrease of its levels by 20% compared with control. Total, $Na^+$-dependent, and $Na^+$-independent glutamate transport increased by 69%, 73%, and 73%, respectively, in 0-μM glutamine compared with control. In the condition of the limited availability of extracellular glutamine, the metabolic pathway via glutamine hydrolysis may not be important for the synthesis of glutathione. Our data that glutamine transport decreased in glutamine-deprived conditions support this concept. For the synthesis of glutathione, SK-N-SH neuroblastoma cells may replace its precursor, glutamate, normally provided by glutamine with glutamate transported through the cell membrane when extracellular glutamine levels are diminished.

In the present study, cell growth rates and biosynthesis of DNA and protein correlated directly with glutamine concentration in culture media. $^3$H-thymidine incorporation decreased by 19%, 41%, and 70% in 400-μM, 200-μM, and 0-μM glutamine, respectively, compared with control. These results are identical with those of our previous study in adult cancer cell lines [3]. Therefore, the response observed in the present study may not be specific to neuroblastoma cells. As shown in Fig. 1, SK-N-SH cells could survive and even grow in glutamine concentrations lower than normal circulating levels (500–600 μM). The centers of solid tumors are generally poorly vascularized, and intercellular amino acid concentrations can be much lower than the normal circulating levels [18]. Our findings obtained from an *in vitro* cell culture model may not be the same as those observed *in vivo*. However, decreased extracellular amino acid levels encountered by tumors *in vivo* may elicit similar adaptive responses in amino acid transport and glutathione synthesis that contribute to the maintenance of cytoplasmic amino acids and glutathione levels.

Collectively, our results, as presented here, support the concept that glutamine mediates neuroblastoma cell proliferation by regulating glutathione synthesis and amino acid transport across the cell membrane, both when sufficient nutrients are available and when key nutrients are in short supply. This mechanism may allow neuroblastoma cells to continue to grow even in tumor tissues that are deprived of nutrients.

## References


1. Medina MA, Sanchez-Jimenez F, Marquez J, et al. (1992) Relevance of glutamine metabolism to tumor cell growth. Mol Cell Biochem 113:1–15
2. Fischer CP, Bode BP, Souba WW (1998) Adaptive alterations in cellular metabolism with malignant transformation. Ann Surg 227:627–636
3. Wasa M, Bode BP, Abcouwer SF, et al. (1996) Glutamine as a regulator of DNA and protein biosynthesis in human solid tumor cell lines. Ann Surg 224:189–197
4. Lusini L, Tripodi SA, Rossi R, et al. (2001) Altered glutathione anti-oxidant metabolism during tumor progression in human renal-cell carcinoma. Int J Cancer 91:55–59
5. Meister A (1991) Glutathione deficiency produced by inhibition of its synthesis, and its reversal; applications in research and therapy. Pharm Ther 51:155–194
6. Carretero J, Obrador E, Anasagasti MJ, et al. (1999) Growth-associated changes in glutathione content correlate with liver metastatic activity of B16 melanoma cells. Clin Exp Metastasis 17:567–574
7. Collins CL, Wasa M, Souba WW, et al. (1998) Determinations of glutamine dependence and utilization by normal and tumor-derived breast cell lines. J Cell Physiol 176:166–178
8. Abcouwer SF, Behrens E, Lustig RJ, et al. (1997) Stress responses to glutamine starvation in human breast cell lines. Proc. Am. Assoc. Cancer Res 38:543
9. Suarez A, Hartmann O, Vassal G, et al. (1991) Treatment of stage IV-S neuroblastoma: a study of 34 cases treated between 1982 and 1987. Med Ped Oncol 19:473–477
10. Gazzola GC, Dall'Asta V, Franchi-Gazzola R, et al. (1981) The cluster tray method for rapid measurement of solute fluxes in adherent cultured cells. Anal Biochem 115:368–374
11. Smith PK, Krohn RI, Hermanson GT, et al. (1985) Measurement of protein using bicinchoninic acid. Anal Biochem 150:76–85
12. Wasa M, Bode BP, Souba WW (1996) Adaptive regulation of amino acid transport in nutrient-deprived human hepatomas. Am J Surg 171:163–169
13. Low SY, Rennie MJ, Taylor PM (1994) Sodium-dependent glutamate transport in cultured rat myotubes after glutamine deprivation. FASEB J 8:127–131
14. Kilberg MS, Han HP, Barber EF, et al. (1985) Adaptive regulation of neutral amino acid transport system A in rat H4 hepatoma cells. J Cell Physiol 122:290–298
15. Wasa M, Wang HS, Tazuke Y, et al. (2001) Insulin-like growth factor-I stimulates amino acid transport in a glutamine-deprived human neuroblastoma cell line. Biochim Biophys Acta 1525:118–124
16. Obrador E, Navarro J, Mompo J, et al. (1997) Glutathione and the rate of cellular proliferation determine tumour cell sensitivity to tumour necrosis factor in vivo. Biochem J 325:183–189
17. Mickisch G, Fajta S, Bier H, et al. (1991) Cross-resistance patterns related to glutathione metabolism in primary human renal cell carcinoma. Urol Res 19:99–103
18. Shotwell MA, Kilberg MS, Oxender DL (1983) The regulation of neutral amino acid transport in mammalian cells. Biochim Biophys Acta 737:267–284

Available online at www.sciencedirect.com
SCIENCE DIRECT®
Health Policy 73 (2005) 52–57
HEALTH policy
www.elsevier.com/locate/healthpol

# Actual and estimated costs of disposable materials used during surgical procedures

Shin-ichi Toyabe[a,*], Pengyu Cao[a], Sachiko Kurashima[a], Yukiko Nakayama[b], Yuko Ishii[b], Noriko Hosoyama[b], Kouhei Akazawa[a]

[a] *Department of Medical Informatics, Niigata University Medical and Dental Hospital, Asahimachi-dori 1-754, Niigata 951-8520, Japan*
[b] *Operating Department, Niigata University Medical and Dental Hospital, Niigata, Japan*

**Abstract**

It is difficult to estimate precisely the costs of disposable materials used during surgical operations. To evaluate the actual costs of disposable materials, we calculated the actual costs of disposable materials used in 59 operations by taking account of costs of all disposable materials used for each operation. The costs of the disposable materials varied significantly from operation to operation (US$ 38–4230 per operation), and the median [25-percentile and 75-percentile] of the sum total of disposable material costs of a single operation was found to be US$ 686 [205 and 993]. Multiple regression analysis with a stepwise regression method showed that costs of disposable materials significantly correlated only with operation time ($p < 0.001$). Based on the results, we propose a simple method for estimating costs of disposable materials by measuring operation time, and we found that the method gives reliable results. Since costs of disposable materials used during surgical operations are considerable, precise estimation of the costs is essential for hospital cost accounting. Our method should be useful for planning hospital administration strategies.


*Keywords:* Hospital resources; Cost sharing

## 1. Introduction

Since many kinds of disposable materials are used during operations, it is difficult to estimate precisely the costs of these materials [1,2]. The costs of disposable materials such as gauzes, needles and strings, which are used in large numbers, are particularly difficult to calculate. The costs of these disposable materials are usually allocated to operations from total costs of disposable materials used in the operation department [3]. However, this method is based on the incorrect assumption that the same amounts of disposable materials are used during operation regardless of the kind of operation.

The objective of this study was to evaluate the precise costs of disposable materials used during operations and to develop a method to estimate precisely the costs of disposable materials used during an operation. To calculate actual costs of disposable materials used during each operation, we recorded lists of all

* Corresponding author. Tel.: +81 25 227 2472; fax: +81 25 227 0850.
*E-mail address:* toyabe@med.niigata-u.ac.jp (S.-i. Toyabe).

0168-8510/$ – see front matter © 2004 Elsevier Ireland Ltd. All rights reserved.
doi:10.1016/j.healthpol.2004.10.003

disposable materials used during the operation. The results showed that the costs of disposable materials varied from operation to operation and that the total cost of disposable materials is considerable. Although this method gives precise results, it is too time-consuming [1,2,4]. A more practical method is needed for calculation of material costs of each operation [5,6]. We developed a more practical method to calculate costs of medical materials used during operations [3,7].

## 2. Materials and methods

A flowchart of the method of analysis used in this study is shown in Fig. 1. The analysis was divided into three steps: collection of cost data, identification of cost allocation factors, and comparison of actual costs with estimated costs. Each of these steps is explained in detail below.

### 2.1. Collection of cost-related data

Cost-related data for the eleven factors in step 1 in Fig. 1 were collected in 59 operations during the period from July to October in 2003. The 11 factors were (1) patient background, (2) operation method, (3) disposable material costs, (4) number of disposable materials, (5) operation time, (6) number of staff and (7) anesthesia method. Table 1 shows the surgical procedures used.

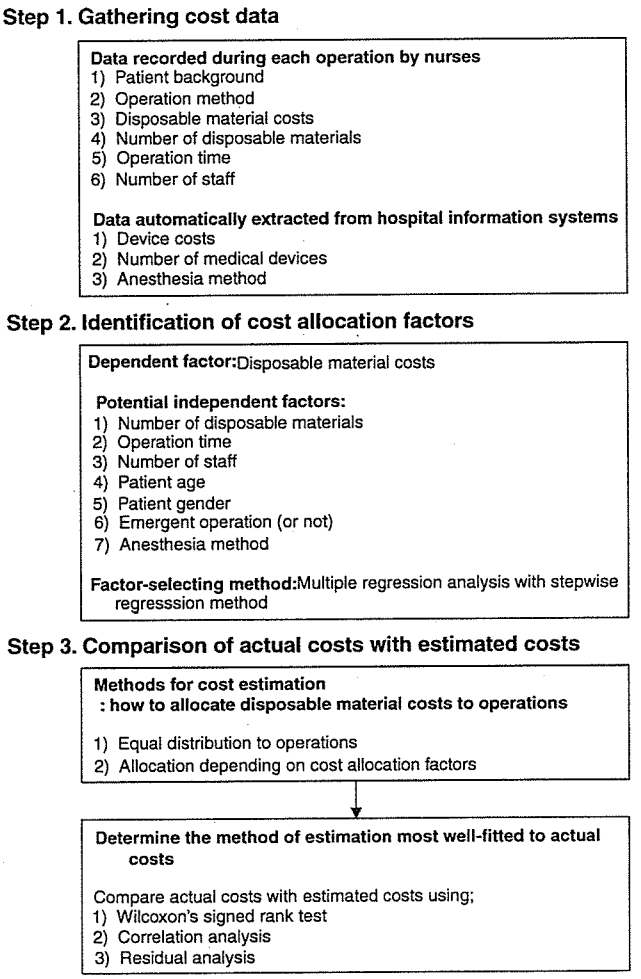


Fig. 1. Analysis flowchart.

Table 1
List of surgical procedures

| Operation | Number of cases |
|---|---|
| Bilateral pediatric inguinal herniotomy | 1 |
| Cataract operations plus intraocular lens inplantation | 3 |
| Cerebral revasculization | 2 |
| Glaucoma operation (goniotomy) plus intraocular lens inplantation | 2 |
| Glaucoma operation (trabeculectomy) | 2 |
| Glaucoma operation (trabeculectomy) plus intraocular lens inplantation | 1 |
| Heart valve replacement | 3 |
| Hepatic segmentectomy | 2 |
| Laparoscopic adnexectomy | 3 |
| Lobar hepatectomy | 1 |
| Pediatric inguinal herniotomy plus hydrocelectomy | 1 |
| Pediatric inguinal herniotomy plus umbilical herniotomy | 2 |
| Renal transplantation | 3 |
| Renal transplantation and splenectomy | 1 |
| Replacement of artificial hip joint | 1 |
| Replacement of artificial hip joint plus autologous bone transplantation | 2 |
| Resection of pancreas head | 1 |
| Resection of pancreas head plus arterioplasty | 1 |
| Resection of rectal cancer | 2 |
| Resection of rectal cancer plus cholecystectomy | 1 |
| Strabismus surgery | 2 |
| Thoracoscopic lobectomy | 3 |
| Total colectomy | 2 |
| Total gastrectomy | 5 |
| Transurethral prostate biopsy | 2 |
| Tympanoplasty | 2 |
| Unilateral pediatric inguinal herniotomy | 2 |
| Vitreous surgery | 1 |
| Vitreous surgery plus intraocular lens inplantation | 5 |
| Total | 59 |

To obtain actual cost data, we made a list of all of the medical materials, including materials of low cost such as sheets of gauze, used during each operation. All medical materials used during each operation were recorded by a nurse who did not attend the operation. The number of medical staff who attended the operation, including doctors, nurses and medical engineers, was also recorded. The cost of each disposable material was calculated by adding the price of the material to the cost of maintaining the material handling department. The price data of each material was based on the database supplied University Hospital Medical Information Network (UMIN) [8]. The total costs of maintaining the material handling department were allocated to each material according to the price of the material. Grubbs-Smirnov test was used to detect outliers in the distribution of cost data [9].

### 2.2. , dHntificDtion oI cost D@@cDtion IDctoUs

"Cost allocation factors" are allocation bases utilized for applying costs to services or procedures, resembling cost drivers used in an activity-based costing (ABC) system [7]. We selected cost allocation factors from factors that significantly affect disposable material costs (number of disposable materials, operation time, number of staff, patient age, gender, anesthesia method, emergency operation or not) using multiple regression analysis with a stepwise regression method [10]. All variables were standardized to zero mean and unit variance. The significance level of 0.05 was adopted as the criterion for entering the factors into the regression model, regarding the stepwise method. Univariate regression analysis was performed to study association between cost of disposable materials and each of the factors listed above.

### 2.3. Comparison of actual costs and estimated costs

Generally, cost data of all disposable materials used in an operating room are easily obtained from the hospital information systems. To calculate the disposable material costs in a single operation, the total costs should be distributed to operations in an appropriate manner. The conventional method to allocate total costs of disposable materials to operations is equal distribution to operations [3]. We propose an alternative method: allocation of total costs to each operation based on predetermined cost allocation factors. Wilcoxon's signed rank test was used to compare the actual cost data and the estimated cost data. A $p$-value of less than 0.05 was considered statistically significant. The 'goodness of fit' in each estimation was analyzed by the coefficient of determination and residuals between estimated costs and actual costs. All cost data are expressed in US dollars. The distributions of continuous data were expressed by median [25-percentile

and 75-percentile] or by mean ± standard deviation if appropriate.

## 3. Results

### 3.1. Actual cost data of medical materials used during operations

The actual costs of all disposable materials varied from US$ 38 to US$ 4230, and the median [25-percentile and 75-percentile] cost was US$ 686 [205 and 993]. The number of disposable materials used during an operation differed from 17 to 697, the median [25-percentile and 75-percentile] being 80 [57,165].

### 3.2. s ariances of costs of the same operation

Variances of costs of medical materials in total gastrectomies performed on five patients were examined. The operations were performed by different surgeons, but the patients' backgrounds are the same. The costs of disposable materials used in each operation varied from US$ 948 to US$ 5825 (median, US$ 2875).

### 3.3. o egression analysis of costs of disposable materials

Multiple regression analysis was performed by the stepwise regression method to determine the importance of factors associated with disposable material costs [10]. Operation time was the only factor selected as a significant factor associated with disposable material costs (standardized correlation coefficient of 0.927, $p < 0.001$). Univariate regression analysis showed that operation time was significantly associated with disposable material cost ($o^2 = 0.859$, $p < 0.001$).

### 3.4. Average costs of disposable materials per unit of operation time and per operation

Since disposable material costs were found to depend on operation time, we calculated the average cost per unit of operation time (Fig. 2). The costs per unit of operation time were almost constant in all but two operations. The costs of those two operations were much higher than those for other operations and were shown to be outliers by the Grubbs-Smirnov test ($p < 0.01$) [9]. They were cataract operations plus intraocular lens implantation, and the reason for the high costs of these operations is the high costs of intraocular lenses. The disposable material cost per operation time was US$ 3.2/min [2.2, 3.9] based on data for 57 operations, whereas it was US$ 3.70/min calculated by total costs and sum of operation times for the operations performed in the operating room in our hospital in 2003. The disposable material cost per operation was calculated to be US$ 459.3.

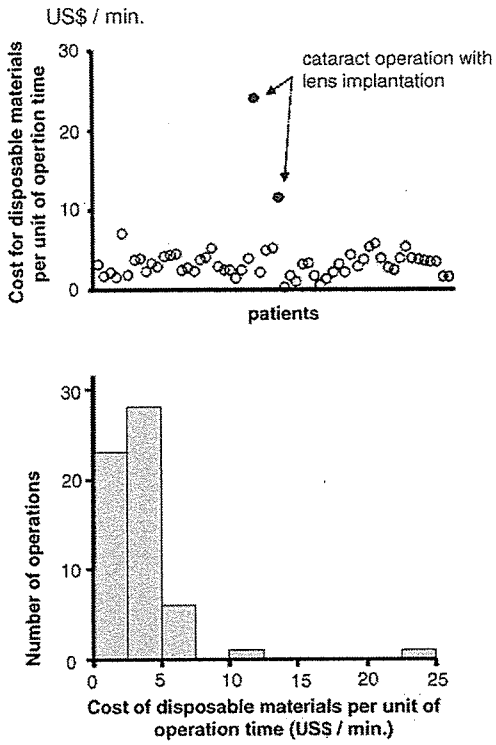


Fig. 2. Disposable material costs per unit of operation time in each operation. Two operations were shown to be outliers by the Grubbs-Smirnov test ($p < 0.01$, closed circles).

### 3.5. Estimated costs of medical materials used during each operation

Based on the results of multiple regression tests, we estimated costs of disposable materials by allocating to each operation equally (conventional method) and by allocating to each operation according to operation time. The costs estimated by these methods were compared with the actual costs in 57 operations (Table 2). The actual costs were significantly different from the

Table 2
Comparison of costs of disposable medical materials used during operations estimated by two different methods

| Methods for estimation of cost of disposable materials | Comparison with actual cost ($p$)[a] | Coefficient of determination ($o^2$)[b] | Residual between estimated and actual costs[c] |
|---|---|---|---|
| 1. Equal distribution to operation | 0.001 | – | −365.2 ± 814.5 |
| 2. Cost allocation in proportion to operation time | 0.062 | 0.927 ($p<0.001$) | 88.6 ± 306.3 |

[a] Wilcoxon's signed rank test was used to examine differences between actual costs and estimated costs.
[b] Pearson's correlation test was used to examine correlation between actual costs and estimated costs.
[c] Residual between estimated costs and actual costs is expressed as mean ± S.D.

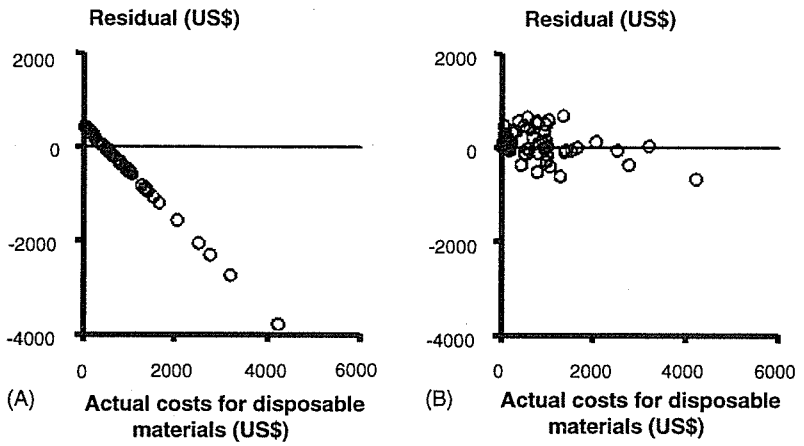


Fig. 3. Relationship between the actual costs of disposable materials used during operations and the residuals that were estimated costs minus actual costs. The estimated costs were calculated by the conventional method, in which costs were allocated equally to operations (A), and by our method, in which costs were allocated to operations according to operation time (B).

costs estimated by the conventional method ($p=0.001$). The costs estimated by our method, on the other hand, agreed well with the actual costs. The average residual between the actual costs and the costs estimated by our method was smaller than that estimated by the conventional method (Fig. 3).

## 4. Discussion

Current status of disposable material costs is not obvious, because it is not exactly known what materials are used for an individual patient [11,12]. Our results demonstrate that the disposable material costs per operation are considerable and vary significantly from operation to operation. Therefore, precise calculation of disposable materials used for each operation is essential to know the precise costs per operation and to reduce variance between physicians [1,13]. Inappropriate allocation of disposable material costs would result in the adoption of erroneous strategies for hospital management.

Since calculation of disposable material costs by adding the costs of all materials is a precise but time-consuming method [1], other methods to allocate total costs of disposable materials to operations are needed [3,6,7,14,15]. The costs of disposable materials have been calculated by allocating the costs equally to operations. However, our results demonstrate that cost data estimated by the conventional method differ significantly from actual cost data (Table 2). We determined the factors that significantly affect costs of disposable materials by using multiple regression analysis to ascertain the cost allocation factors. The results revealed that the only factor regressed with disposable material costs was operation time. We therefore proposed a simple method for estimating the costs of each operation based on regression using operation time as an

explanatory variable. Our method for estimating costs of disposable materials is simple, more reliable than previous methods, and applicable to most operations except for some outliers (Fig. 2). Our method should be useful for planning hospital administration strategies.

## References


[1] Allen JW, Polk Jr HC. A study of added costs of laparoscopic cholecystectomy based on surgery preference cards. The American Surgeon 2002;68:474–6.

[2] Adachi Y, Shiraishi N, Ikebe K, Aramaki M, Bandoh T, Kitano S. Evaluation of the cost for laparoscopic-assisted Billroth I gastrectomy. Surgical Endoscopy 2001;15:932–6.

[3] Udpa S. Activity cost analysis: a tool to cost medical services and improve quality of care. Management Care Quarterly 2001;9:34–41.

[4] Udpa S. Activity-based costing for hospitals. Health Care Management Review 1996;21:83–96.

[5] Austin PC, Ghali WA, Tu JV. A comparison of several regression models for analysing cost of CABG surgery. Statistics in Medicine 2003;22:2799–815.

[6] West TD, Balas EA, West DA. Contrasting RCC, RVU, and ABC for managed care decisions. A case study compares three widely used costing methods and finds one superior. Healthcare Finance Management 1996;50:54–61.

[7] Baker JJ, Boyd GF. Activity-based costing in the operating room at Valley View Hospital. Journal of Health Care Finance 1997;24:1–9.

[8] UMIN. See http://www.umin.ac.jp/practice/pharmaceuticals/ (in Japanese). Last checked September 20, 2004.

[9] Stefansky W. Rejecting outliers in factorial designs. Technometrics 1972:14469–79.

[10] Johnson RA, Wichern DW. Applied multivariate statistical analysis. Englewood Cliffs, NJ: Prentice Hall; 1992.

[11] Bertges DJ, Zwolak RM, Deaton DH, Teigen C, Tapper S, Koslow AR, et al. Current hospital costs and medicare reimbursement for endovascular abdominal aortic aneurysm repair. Journal of Vascular Surgery 2003;37:272–9.

[12] Oliver A. Health economic evaluation in Japan: a case study of one aspect of health technology assessment. Health Policy 2003;63:197–204.

[13] Welcker K, Marian P, Thetter O, Siebeck M. Cost and quality of life in thoracic surgery—a health economic analysis in a German center. Thoracic and Cardiovascular Surgery 2003;51:260–6.

[14] Lievens Y, van den Bogaert W, Kesteloot K. Activity-based costing: a practical model for cost calculation in radiotherapy. International Journal of Radiation Oncology, Biology, Physics 2003;57:522–35.

[15] DesHarnais Castel L, Bajwa K, Markle JP, Timbie JW, Zacker C, Schulman KA. A microcosting analysis of zoledronic acid and pamidronate therapy in patients with metastatic bone disease. Support Care Cancer 2001;9:545–51.

Hiroshima J. Med. Sci.
Vol. 54, No. 1, 9~20, March, 2005
**HIJM** 54–2

# Multi-target Models and their Application to Data Analysis of Cellular Mortality due to Radiation Exposure

I Made ARCANA[1] and Megu OHTAKI[2]

*1) Graduate School of Biomedical Sciences, Hiroshima University, 1–2–3 Kasumi, Minami-ku, Hiroshima 734–8551, Japan*

*2) Department of Environmetrics and Biometrics, Research Institute for Radiation Biology and Medicine, Hiroshima University, 1–2–3 Kasumi, Minami-ku, Hiroshima 734–8551*

## ABSTRACT

We consider multi-target models for use in analyzing data of the dose-response relationship. The target sizes we are concerned with here are both homogeneous, as assumed in the classical model, and heterogeneous, as simplified using geometric progression. We apply two models for establishing the multi-target models: a Poisson regression model constructed by assuming that the response variable $Y$ follows Poisson distribution, and a gamma-frailty model as a Poisson mixture model derived by adding random common risks having a gamma distribution. Applying these models to experimental data relating the effects of miso fermentation-stages on the survival rate of cells of intestinal crypts of mice exposed to radiation yielded the result that there were substantial frailties associated with all miso fermentation-stages. Short-term and medium-term fermented miso provided similar effects, whereas long-term fermentation had the lowest relative risk value, indicating a significant protection of the crypts against exposure effects. A gamma-frailty model based on heterogeneous target size was more suitably applied when there were at least 3 dead stem cells having 10 target genes.

***Key words:*** *Gamma-frailty model, Miso (fermented soy bean paste), Poisson regression model, Radio protective effects*

For more than fifty years, the multi-stage model proposed by Armitage and Doll[1] has continued to influence biomedical thinking on cellular changes, particularly in regard to the processes underlying carcinogenesis (e.g., see 2, 15, 17, 21, and 23). This model, however, is derived according to a probabilistic mechanism that is precisely described on the basis of reasonable assumptions[23], of which correspondence to actual events in biomedical fields has not been established. Therefore, Moolgavkar[15] noted that the multi-stage model needs to be embellished in various ways to accommodate our current thinking on carcinogenesis.

Building on the idea of removing stages from the multi-stage model of cell changes, the purpose of the present paper is to establish mathematical models for examining the relation of the dose response level of exposure to cellular changes on the pathway to cell death. These dose-response-based models, called multi-target models, consider a unit in exposed cells as a target.

Survival curves for most mammalian cells exposed to low-LET radiation, such as gamma and X-rays, show a shoulder-shaped curvature, in which there is less cell inactivation per unit dose at the initial low dose region and a tendency towards a constant slope at the higher dose. This constant final slope is caused by the effect of the repair of DNA single strand breaks during exposure. The shoulder region of the curve can be interpreted in two possible ways. Firstly, the given dose is considered as a total of dose fractions that are individually capable of repairing sub-lethal damage in between them[15], but become lethal damage when added together. In this situation, we assume that each dose fraction is given acutely and that the repair of the single strand breaks during the radiation can be ignored. Secondly, lesions are individually reparable, but when the efficiency of the enzymatic repair mechanisms diminishes due to the number of lesions, they are become irreparable and kill the cell. This means that it requires more than two targets getting exposure to radiation on the pathway to cell death. For these reasons, we applied multi-target models to cellular mortality due to radiation exposure.

Suppose that the probability of a target surviving after exposure at dose $D$ is expressed by the survival function $S(D\,|\,\beta)=e^{-\beta D}$, where $\beta$ is an unknown parameter describing the coefficient of exposure effects. Under such a condition, the probability of a target having vital damage is denoted by the failure distribution[12] $F(D\,|\,\beta)=1-e^{-\beta D}$. In the classical multi-target model, it is assumed that

lethal damage occurs after independent hits on a certain number of targets (say $k$), and that the target size is homogeneous. Here, the target size is related to its sensitivity level to radiation effects. The larger the target sizes the higher probability of it getting hit when exposed to radiation. The target survivor function is thus

$$S_k(D|\beta) = 1 - (1 - e^{-\beta D})^k. \quad (1)$$

However, the assumption of homogeneous target size is sometimes unrealistic. It is therefore appropriate to remove this assumption. A general extension of the target survivor function shown in equation (1) that allows each hit target to have a different exposure effect can be formulated by

$$S_k(D|\beta_1, \ldots, \beta_k) = 1 - \prod_{j=1}^{k}(1 - e^{-\beta_j D}), \quad (2)$$

where (unknown) parameter $\beta_j$ represents the coefficient of sensitivity for the $j$-th target, $j$=1, 2, ... , $k$.

For establishing the multi-target models, we apply two models: a Poisson regression model constructed by assuming that the response variable $Y$ follows Poisson distribution, and a gamma-frailty model as a Poisson mixture model derived by adding random common risks having a gamma distribution.

## MULTI-TARGET MODELS

### 1. Geometric Structure on Heterogeneous Targets

By assuming that the parameter of the sensitivity coefficient for the $j$-th target ($\beta_j$) in classical theorem has regularity following geometrical progression, we constructed one of the simplest models for heterogeneity. That is, assume that $\beta_j=\beta\rho^{j-1}$, where the unknown parameter $\rho$ describes the index of heterogeneity of the target size. Then, the survival function in equation (2) can be specified as

$$S_k(D|\beta, \rho) = 1 - \prod_{j=1}^{k}(1 - e^{-\beta\rho^{j-1}D}). \quad (3)$$

From a graphical point of view, in the case that the number of targets $k$=10 for a given exposure dose ($D$), the heterogeneity index value of $\rho$>1 provides significant decreases in the survival curve as compared with that of $\rho$=1, as shown in Fig. 1. Continued increases in the value of $\rho$ may give accelerated increases in the hazard rate.

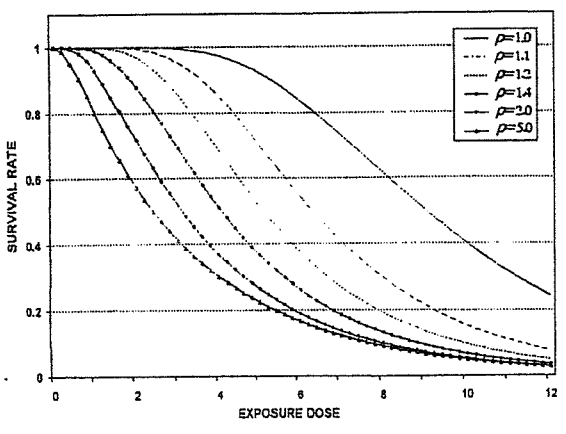


**Fig. 1.** Survival curves of the multi-target models at various values of $\rho$ and given exposure dose ($D$), in a case where the number of targets $k$ is equal to 10 and where the coefficient of exposure effects ($\beta$) is fixed. Significant decreases in the survival curve can be seen when the index value of $\rho$ is greater than 1. A steady increase in the value of $\rho$ results in an accelerated increase in the hazard rate.

### 2. Poisson Regression Model

Let $Y$ be a response variable following Poisson distribution with mean $\mu_k(D, \boldsymbol{x}|\theta^*)=\mu_0 S_k(De^{\gamma^T\boldsymbol{x}}|\beta, \rho)$, a function of exposure dose ($D$) for given covariates vector $\boldsymbol{x}$ and unknown parameters vector $\theta^*=(k, \mu_0, \beta, \rho, \gamma^T)^T$, where $\mu_0$ denotes the baseline mean parameter and $S_k(De^{\gamma^T\boldsymbol{x}}|\beta, \rho)$ expresses the survival function, which is specified as

$$S_k(De^{\gamma^T\boldsymbol{x}}|\beta, \rho) = 1 - \prod_{j=1}^{k}(1 - e^{-\beta\rho^{j-1}De^{\gamma^T\boldsymbol{x}}}), \quad (4)$$

where $\gamma^T\boldsymbol{x} = \gamma_1 x_1 + \gamma_2 x_2 + \cdots + \gamma_p x_p$ is a linear combination of $p$ covariates. Then,

$$P(y|D, \boldsymbol{x}, \theta^*) = \frac{\{\mu_k(D, \boldsymbol{x}|\theta^*)\}^y}{y!} e^{-\mu_k(D,\boldsymbol{x}|\theta^*)}. \quad (5)$$

Given a set of $n$ independent samples $(y_i, D_i, \boldsymbol{x}_i)$, $i$=1,2, ... , $n$, where $y_i$ is the observed response, $D_i$ is the exposure dose and $\boldsymbol{x}_i=(x_{i1}, x_{i2}, \ldots, x_{ip})^T$ is the covariates vector for the $i$th individual, we denote the actually observed data set by $\boldsymbol{d}_{(obs)}=(\boldsymbol{y}, D, \boldsymbol{x}^T)^T$. Then, the likelihood function for estimating the unknown parameters based on the observed data set can be specified by

$$L(\theta^*|\boldsymbol{d}_{(obs)}) = \prod_{i=1}^{n} P(y_i|D_i, \boldsymbol{x}_i, \theta^*). \quad (6)$$

### 3. Gamma-frailty Model for Heterogeneous Background

It is important to take account of heterogeneity between individuals in population-based survival studies[9]. A systematic way of describing heterogeneity is by entering an unobserved quantity called frailty, here denoted by the letter $Z$. This quantity describes common risk factors, measurable or non-measurable, and is not included in the model[9,10,22].

Till now, most studies have used a frailty having a gamma distribution, which is mathematically convenient. Gamma distributions have been used for many years to generate a Poisson mixture model. From a computational point of view, they fit